Anisotropic optical conductivity and two colors of MgB$_2$

V. Guritanu, A. B. Kuzmenko, and D. van der Marel

DPMC, University of Geneva, 24, Quai E.-Ansermet, 1211 Geneva 4, Switzerland

S. M. Kazakov, N. D. Zhigadlo, and J. Karpinski

Solid State Physics Laboratory, ETH 8093 Zurich, Switzerland

(Received 13 September 2005; published 17 March 2006)

We present the anisotropic optical conductivity of MgB$_2$ between 0.1 and 3.7 eV at room temperature obtained on single crystals of different purity by spectroscopic ellipsometry and reflectance measurements. The bare (unscreened) plasma frequency ω_p is almost isotropic and equal to 6.3 eV, which contrasts some earlier reports of a very small value of ω_p. The data suggests that the σ bands are characterized by a stronger electron-phonon coupling λ_{tr} but smaller impurity scattering γ_{imp}, compared to the π bands. The optical response along the boron planes is marked by an intense interband transition at 2.6 eV, due to which the reflectivity plasma edges along the a and c axes are shifted with respect to each other. As a result, the sample spectacularly changes color from a blueish-silver to the yellow as the polarization is rotated from the in-plane direction toward the c axis. The optical spectra are in good agreement with the published *ab initio* calculations. The remaining discrepancies can be explained by the relative shift of σ bands and π bands by about 0.2 eV compared to the theoretical band structure, in agreement with the de Haas-van Alphen experiments. The widths of the Drude and the interband peaks are both very sensitive to the sample purity.

PACS number(s): 74.25.Gz, 74.25.Jb, 78.20.−e, 78.20.Ci

I. INTRODUCTION

The discovery of superconductivity in MgB$_2$ (Ref. 1) caused an excitement in the physics community not only due to an unprecedentedly high T_c ($\sim$40 K) for a "conventional" electron-phonon superconductor, but also because it clearly shows the existence of two distinct gaps;[2] an intriguing phenomenon that, although addressed theoretically, had been never observed before. Magnesium diboride consists of graphitelike boron planes intercalated with Mg atoms. The metallic properties are determined by two distinct types of electronic bands: The strongly covalent almost two-dimensional (2D) σ bands formed by the hybridized sp_xp_y B orbitals and 3D π bands made of p_z orbitals. The holes in the σ bands are strongly coupled to the in-plane bond-stretching phonon modes, giving rise to a high electron-phonon coupling constant.[3] A remarkable implication of such a strong conduction band disparity is a multigap superconductivity: A large gap value on σ bands and a small one on π bands. Notably, the community has enjoyed a rapid advance in understanding the electronic structure and superconducting scenario of MgB$_2$, in contrast to the lengthy siege of the high-T_c problem in the cuprates.

The early theoretical predictions of the electronic structure and the superconducting properties were soon confirmed by the isotope effect,[4,5] angle-resolved photoemission,[6] de Haas-van Alphen (dHvA),[7] specific heat,[8–10] tunneling measurements,[11] and, recently, by the inelastic x-ray scattering.[12] Even though the far-infrared experiments[13–18] have clearly shown the lowest of the superconducting gaps in agreement with the theory and other spectroscopic probes, the optical measurements so far demonstrated a rather poor reproducibility and equally poor consistency with the theoretical electronic structure. The most controversial issue is

value of the Drude plasma frequency ω_p. While the theory predicts a high value of ω_p of $\approx$7 eV, which corresponds to about one conducting electron per unit cell, a number of groups[14,19–23] reported a much smaller value of about 1.5–2.5 eV, corresponding to 0.15 electrons per cell. In Ref. 20, in addition to the narrow Drude peak, a broad continuum, which could contain the missing Drude spectral weight, was found below 1 eV. However, the existence of such a continuum was not reliably verified by other groups. Another inconsistency is related to the anisotropy of the plasma frequency. The calculations provide very close (within 5%) values of $\omega_{p,a}$ and $\omega_{p,c}$, which should be regarded, in fact, as a coincidence, because the plasma frequency of the carriers in the 2D σ bands is strongly anisotropic. A study of the optical anisotropy of magnesium diboride was undertaken by Fudamoto and Lee[23] by the comparison of the reflectivity spectra measured on a mosaic of ab-oriented crystals and on a polycrystalline sample. They observed the in-plane reflectivity plasma edge at about 16 000 cm^{-1}. The authors also suggested that an additional structure in the reflection of a polycrystal is due to the c-axis plasma edge at 22 000 cm^{-1}. Thus the anisotropy ratio $\omega_{p,a}/\omega_{p,c} \approx 0.73$ was deduced, which is in contrast with the theoretical prediction.

The optically derived electron-phonon coupling constant λ_{tr} was also a subject of debate.[19,22,24,25] Values of λ_{tr} ranging from 0.13 (Ref. 19) to 1.5 (Ref. 22) were reported. It was pointed out in Ref. 25 that the determination of λ_{tr} relies strongly on the plasma frequency, which is not yet well established. One should keep in mind that different values of the coupling constant for the σ and π bands are expected from the calculations[3] and observed in the dHvA experiment.[7]

With a lack of large single crystals of MgB$_2$, especially along the c axis, the optical measurements were done on polycrystalline samples,[18,20,23] disoriented,[22,26] or
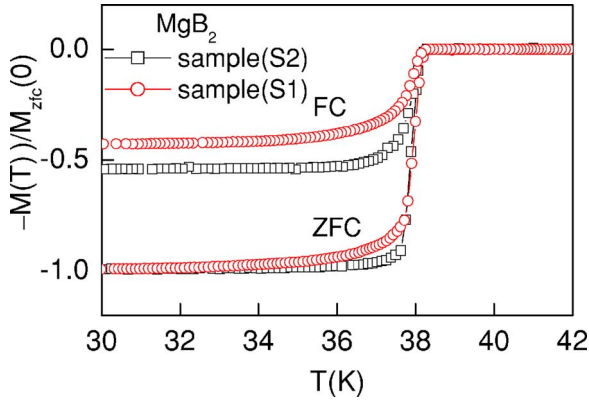
FIG. 1. (Color online) Magnetization measurements of the superconducting transition of the two single crystals of MgB$_2$ used in this paper.

ab-oriented[15,16,19] films as well as *ab*-oriented crystal mosaics.[17,23] We believe that a large spread of the published optical results can be explained by (i) different purity levels of the samples used, (ii) experimental difficulties to extract the anisotropic complex conductivity from the standard measurements on such objects, and (iii) a fast rate of the surface degradation in air.[20,23]

In this work, we do optical experiments on individual freshly polished single crystals of different purity having no contact with the air. The real and imaginary parts of the in-plane and out-of-plane optical conductivities are derived from the reflectivity and ellipsometry measurements on the *ab*- and on the *ac*-oriented crystals. The measurements show a large (≈ 6.3 eV) and almost isotropic plasma frequency. We find different positions of the reflectivity plasma edges for the two light polarizations. However, such anisotropy is due to extra screening of charge carriers by an interband transition at 2.6 eV, optically active along the *ab* plane, rather than the anisotropy of the bare plasma frequency itself. The anisotropic spectra are in satisfactory agreement with the first-principles calculations of the band structure and the electron-phonon interaction. We discuss the possible corrections to the electronic structure which follow from the optical results.

Finally, the presented data tell us what is the "true" color (or rather, colors) of MgB$_2$.

II. SAMPLES AND PREPARATION

High-quality single crystals of MgB$_2$ have been grown using a cubic anvil technique via the peritectic decomposition reaction of the MgNB$_9$ and Mg at temperature up to 2000 °C under a pressure of 30–35 kbar. The details of the crystal growth and extensive characterization are given elsewhere.[27] The measurements were done on two samples, referenced below as $S1$ and $S2$. The samples were grown under slightly different conditions. For the sample $S1$ the purity of Mg was 99.8%, while a 4N-pure (99.98%) magnesium was used in the second case. The maximum temperature of crystal growth was higher for the sample $S2$ by about 80 °C. The time at the highest temperature was 10 min for

the first sample and 30 min for the second one. The T_c of both samples is close to 38 K (see Fig. 1), although sample $S2$ shows a somewhat narrower transition and a larger field-cooled diamagnetic signal compared to the one of $S1$. The dimensions ($a \times b \times c$) of the as-grown crystals were $0.7 \times 0.5 \times 0.27$ mm^3 for $S1$ and $0.6 \times 0.5 \times 0.18$ mm^3 for $S2$. We selected a thicker sample $S1$ to prepare the (ac) optical face, while sample $S2$ was used to measure on the (ab) face. The faces were dry polished using a 0.1 μm diamond abrasive, since the as-grown surfaces were not suitable for quantitative optical examination.

As it was noticed before,[20,23] the exposed surface of MgB$_2$ deteriorates quickly, largely due to the air moisture. In order to avoid the contamination, the samples were kept in a flow of dry nitrogen during and after the polishing until the end of the measurements. With this precaution, the optical characteristics did not change noticeably during the experiment. On the other hand, switching off the flow immediately affected the optical signal, as shown in the Appendix .

III. OPTICAL EXPERIMENT AND RESULTS

Optical properties of MgB$_2$ at room temperature were obtained using spectroscopic ellipsometry at 0.75–3.7 eV and the reflectivity measurements in the infrared range from 0.1 to 0.85 eV. In all experiments, the sample was mounted on top of a cone and aligned with a laser.

The high-frequency spectra were collected using the Woollam VASE32 ellipsometer while the sample was kept in a flow of dry nitrogen. The in-plane $\epsilon_a(\omega) = \epsilon_{1,a}(\omega) + 4\pi i \sigma_{1,a}(\omega)/\omega$ and the c axis $\epsilon_c(\omega) = \epsilon_{1,c}(\omega) + 4\pi i \sigma_{1,c}(\omega)/\omega$ components of the complex dielectric tensor were both extracted directly from the measurements on the ac surface of the sample $S1$, using two orthogonal crystal orientations and three angles of incidence. For the sample $S2$, only the in-plane optical functions $\epsilon_{1,a}(\omega)$ and $\sigma_{1,a}(\omega)$ were derived from the measurement on the ab plane, using the c axis data from the sample $S1$ to correct for the admixture of the out-of-plane component. The details of the recovery of $\epsilon_a(\omega)$ and $\epsilon_c(\omega)$ from the ellipsometric output are given in the Appendix .

The reflectivity $R(\omega)$ was measured with a polarizer in the range 0.1–0.85 eV at a near-normal angle of incidence using a Fourier transform spectrometer Bruker 66v. The sample was inside a vacuum chamber of a cryostat. A gold layer was sputtered *in situ* on the crystal surface to get a reference signal. We reconstructed the full reflectivity spectrum using the ellipsometrically determined dielectric functions in the optical range

$$R_\nu(\omega) = \left| \frac{1 - \sqrt{\epsilon_\nu(\omega)}}{1 + \sqrt{\epsilon_\nu(\omega)}} \right|^2, \quad (\nu = a, c). \quad (1)$$

The spectra from two regions were combined in order to obtain the complex dielectric function in the whole range. While $\epsilon(\omega)$ was measured directly above 0.75 eV, at low frequencies we applied a variational Kramers-Kronig (KK) constrained analysis of the data. In this method, described in Ref. 28, one finds a KK-consistent dielectric function, which
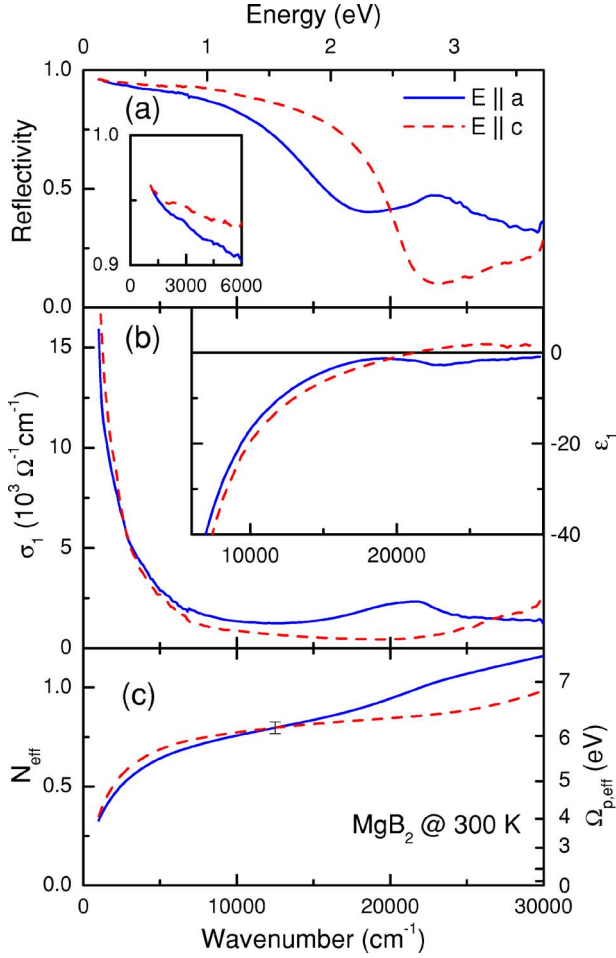
FIG. 2. (Color online) Optical anisotropic spectra of the MgB$_2$ at 300 K derived from the ellipsometry and reflectivity measurements on the sample $S1$ as described in the text: the normal-incidence reflectivity $R(\omega)$(a), optical conductivity $\sigma_1(\omega)$, the dielectric function $\epsilon_1(\omega)$ (b), the effective number of carriers $N_{\text{eff}}(\omega)$, and the effective plasma frequency $\Omega_{\text{p,eff}}(\omega)$ (c). The a axis and the c axis spectra are shown by the solid blue and dashed red lines, respectively.

gives the best detailed match to the reflectivity $R(\omega)$ at low frequencies and both $\epsilon_1(\omega)$ and $\epsilon_2(\omega)$ at high frequencies simultaneously. This procedure allows one to anchor the phase of the complex reflectivity as compared to the usual KK transform.[29] Figures 2(a) and 2(b) show the anisotropic reflectivity $R(\omega)$, optical conductivity $\sigma_1(\omega)$, and the dielectric function $\epsilon_1(\omega)$, measured on sample $S1$. Qualitatively, both in-plane and c-axis spectra exhibit a similar metallic behavior, characterized by a reflectivity plasma edge, a Drude peak in $\sigma_1(\omega)$ and negative $\epsilon_1(\omega)$. However, one can see a strong anisotropy. The in-plane reflectivity shows a broad plasma edge at about 2 eV. The dielectric function $\epsilon_{1,a}(\omega)$ almost reaches zero at the same frequency, but then it varies nonmonotonically while remaining negative at least up to 3.7 eV. In contrast, the c-axis plasma edge is significantly sharper and is higher in energy by about 0.5–0.6 eV. Correspondingly, $\epsilon_{1,c}(\omega)$ behaves monotonically and crosses zero at $\omega_{p,c}^* \approx 2.6$ eV. These results agree with the previous

findings of Fudamoto and Lee[23] who obtained a plasma edge at about 16 000 cm^{-1} (2 eV) on a mosaic of ab-oriented crystals. Although no direct reflectivity measurements for $E\|c$ were reported so far, the same authors suggested[23] that the additional steplike structure at 22 000 cm^{-1} (2.7 eV) in the reflectivity of polycrystals samples comes from the c axis plasma edge. The present study fully confirms this assignment.

The in-plane optical conductivity $\sigma_{1,a}(\omega)$ shows an intense interband peak at ~ 2.6 eV, which is totally absent in the $\sigma_{1,c}(\omega)$ [Fig. 2(b)]. Its origin will be discussed below. Since this peak is close to the screened plasma frequency, it broadens the plasma edge and shifts it to lower frequencies by providing an additional screening of the charge carriers. It is also responsible for a nonmonotonic behavior of $\epsilon_{1,a}(\omega)$ at higher frequencies and even for a structure in $R_a(\omega)$ above 3 eV, which resembles a "second" plasma edge.

Figure 2(c) depicts the partial sum rule (effective number of carriers) function

$$N_{\text{eff}}(\omega) = \frac{2mV_c}{\pi e^2}\int_0^\omega \sigma_1(\omega')d\omega', \qquad (2)$$

where m is the free electron mass, $V_c = 28.9$ Å^3 is the unit cell volume, e is the electron charge, and the corresponding effective plasma frequency

$$\Omega_{\text{p,eff}}(\omega) = \left[8\int_0^\omega \sigma_1(\omega')d\omega' \right]^{1/2}. \qquad (3)$$

Since the integration of $\sigma_1(\omega)$ has to start from zero frequency, while the optical data are taken down to 100 meV, one has to be vigilant about the error bars involved. Fortunately, the fact that the dielectric function obtained by the method used[28] satisfies the KK relations and describes both $\epsilon_1(\omega)$ and $\epsilon_2(\omega)$ at high frequencies poses fairly tight bounds [shown in Fig. 2(c)] on the allowed values of N_{eff}. One can see that at the photon energy of 1.7 eV, which is high enough to comprise most of the intraband spectral weight, but below the interband peak at 2.6 eV, N_{eff} is about 0.8 for both polarizations, which corresponds to a plasma frequency of 6.3 eV. A more rigorous estimate of the ω_p which take into account the broadening of the Drude peak, as described below, gives almost the same value of the plasma frequency (see Table I). This is in contrast with the conclusion of Ref. 23 about a strong anisotropy of the plasma frequency, based on the different positions of the reflectivity plasma edge for the two polarizations. The anisotropy of the reflectivity plasma edge is caused by extra screening due to the in-plane interband transition at 2.6 eV and not by the strong anisotropy of the unscreened plasma frequency.

It is interesting to compare the in-plane optical properties of the two samples ($S1$ and $S2$), which were prepared under different conditions and have presumably slightly different impurity levels (see Fig. 3). One can see that the two most prominent features of the optical conductivity—the Drude peak and the 2.6 eV interband peak—are significantly sharper in sample $S2$. As a result, the reflectivity plasma edge is also sharper and the "double-plasmon" structure in $R_a(\omega)$

TABLE I. Model parameters which give the best match to the measured optical spectra of MgB$_2$ at 300 K and the ratio $\rho_a(300\ \text{K})/\rho_a(40\ \text{K})$ from Ref. 38, as described in the text. Parameters, marked by *, were fixed to the values given by the band calculations.

Parameter	*ab* plane	*c* axis
$\omega_{p,\sigma}$	4.14* eV	0.68* eV
$\omega_{p,\pi}$	4.72 eV	6.31 eV
$\omega_{p,\text{tot}}$	6.28 eV	6.35 eV
$\gamma_{\sigma\text{imp}}$	12.4 meV	
$\gamma_{\pi\text{imp}}$	85.6 meV	
ω_1	2.60 eV	3.92 eV
S_1	1.79	1.7
γ_1	1.11 eV	1.51 eV
ω_2	8.57 eV	-
S_2	6.81	-
γ_2	100.2 eV	-
ϵ_∞	3.31	3.07

is more pronounced than in sample $S1$. One should keep in mind that sample $S2$ was prepared from a more pure magnesium, and it shows a sharper superconducting transition (Fig. 1). This suggests that even a small impurity level (about 0.2% in this case) affects significantly optical and transport properties of MgB$_2$.

The close values of $\epsilon_{1,a}(\omega)$ for the two samples suggest that their in-plane plasma frequencies are similar, although the N_{eff} is slightly higher for sample $S1$, which could be related to a stronger broadening of the interband peaks.

IV. DISCUSSION

A. Extended drude analysis

The extended Drude model has been commonly used to analyze interactions in electronic systems. In this formalism, the frequency dependent scattering rate $1/\tau(\omega)$ and effective mass $m^*(\omega)/m$ are derived from the measured complex dielectric function

$$\frac{1}{\tau(\omega)} = -\frac{\omega_p^2}{\omega} \text{Im}\left(\frac{1}{\epsilon(\omega) - \tilde{\epsilon}_\infty}\right), \quad (4)$$

$$\frac{m^*(\omega)}{m} = -\frac{\omega_p^2}{\omega^2} \text{Re}\left(\frac{1}{\epsilon(\omega) - \tilde{\epsilon}_\infty}\right). \quad (5)$$

The only parameters of this conversion are the total Drude plasma frequency ω_p and the high-frequency dielectric constant $\tilde{\epsilon}_\infty$, due to all contributions other than the conduction electrons. Both $1/\tau(\omega)$ and $m^*(\omega)/m$ have a direct microscopic interpretation in the context of the electron-phonon interaction. One should keep in mind, however, that the model assumes that only one type of carrier contributes to the Drude response. In the case of MgB$_2$, which has two distinct systems of bands (σ and π), the scattering rate and the effective mass obtained by Eqs. (4) and (5) should be
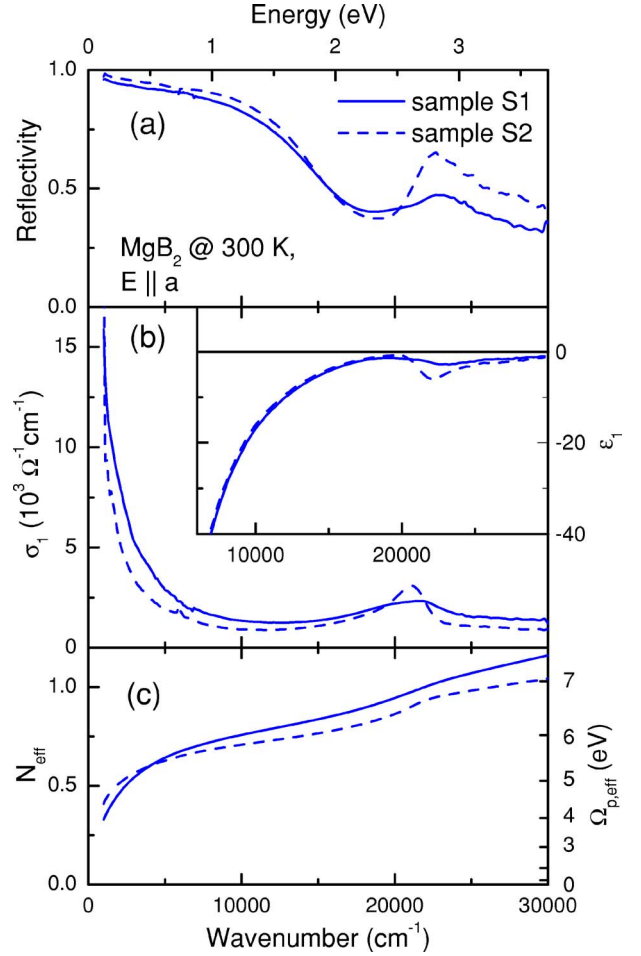

FIG. 3. (Color online) Comparison of the in-plane optical spectra measured on different samples. The same types of spectra are presented as in Fig. 2. The spectra of samples $S1$ and $S2$ are shown by the solid and dashed lines, respectively. Sample $S2$ has presumably a smaller concentration of impurities than sample $S1$.

regarded as an averaged value of contributions from each band. Figure 4 (symbols) shows $1/\tau(\omega)$ and $m^*(\omega)/m$ for the in-plane and the *c*-axis directions, measured on the sample $S1$. We took the values $\omega_{p,a}$=6.28 eV, $\omega_{p,c}$=6.35 eV, $\tilde{\epsilon}_{\infty,a}$=11.9, $\tilde{\epsilon}_{\infty,c}$=4.77, which are suggested by the data fitting in Sec. IV C (see Table I). The value of $\tilde{\epsilon}_\infty$ here is given by the sum of ϵ_∞ in the Table I and the oscillator strengths S_i of the Lorentz oscillators. The solid curves in Fig. 4 were calculated using the results of the fit described in Sec. IV C. One can see that the scattering rate and the mass renormalization are larger for the in-plane direction. It is worth mentioning that the σ bands with a cylinderlike Fermi surface must have a small electromagnetic response along the *c* axis, while the π bands are expected to have comparable contributions in both directions. The present result thus suggests that the electron-phonon coupling is stronger in the σ bands. This is in agreement with the first-principles calculations of Kong *et al.*,[3] who found that the total strength of the electron-phonon interaction is dominated by the coupling of the σ holes to the bond-stretching optical phonons. A quantitative analysis of the electron-phonon interaction must take into account the multiband electronic structure.
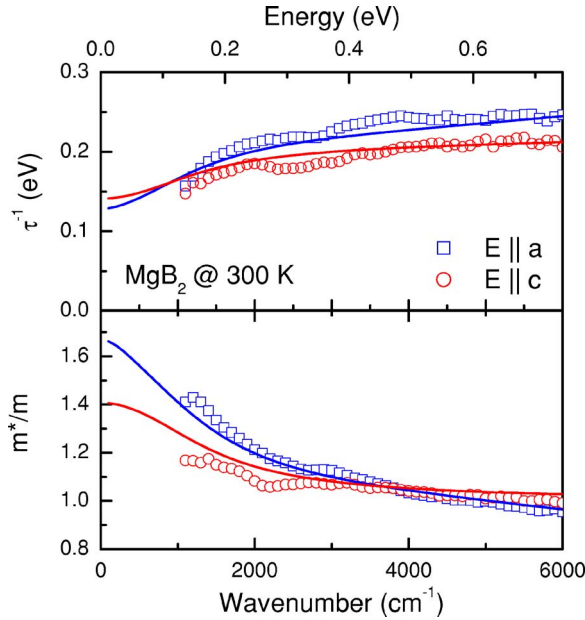
FIG. 4. (Color online) Extended Drude analysis of the optical conductivity of MgB_2 (sample $S1$) at 300 K along the in-plane and the c-axis directions. The symbols are the data, the solid curves show the two-component fit as described in the Sec. IV C.

B. Comparison with *ab initio* calculations

A deeper insight can be attained by the comparison of the optical data with the existing first-principles calculations of the band structure and electron-phonon interaction. One can compute the dielectric function, assuming that the intraband optical conductivity is formed by the additive contributions of carriers in the σ and the π bands. The two bands are characterized by different electron-phonon (Eliashberg) transport functions $\alpha_{tr}^2 F(\omega)$ and impurity scattering rates γ_{imp}. Intraband optical response can be calculated using finite-temperature memory-function formalism for electron-boson interaction.[30] The total conductivity is a sum of the intraband, interband (ϵ^{IB}) and core-electron (ϵ_∞) responses

$$\epsilon_\nu(\omega) = \sum_{\beta=\sigma,\pi} \frac{\omega_{p,\nu\beta}^2}{-\omega[\omega + iM_\beta(\omega,T)]} + \epsilon_\nu^{IB}(\omega) + \epsilon_{\nu\infty}(\nu=a,c).$$

(6)

The contribution of each of the two bands is determined by its respective anisotropic plasma frequency ($\omega_{p,a}$, $\omega_{p,c}$) and the memory function[30]

$$M_\beta(\omega,T) = \gamma_{\beta imp} - 2i\int_0^\infty d\Omega\, \alpha_{tr}^2 F_\beta(\Omega) K\left(\frac{\omega}{2\pi T}, \frac{\Omega}{2\pi T}\right),$$
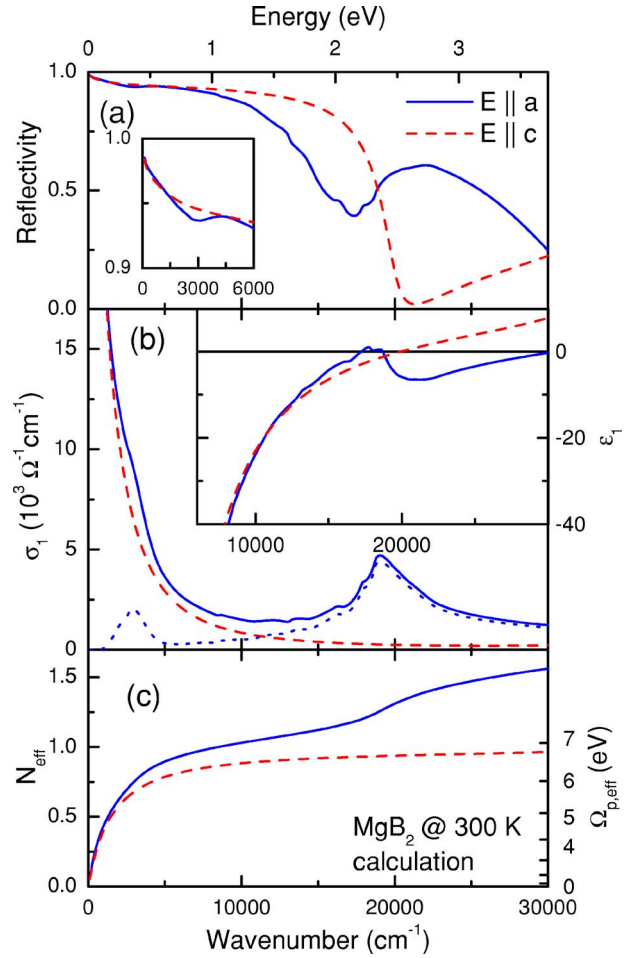
(7)

where

FIG. 5. (Color online) Anisotropic optical spectra of MgB_2 at 300 K, calculated using the results of the published first-principle studies (Refs. 3 and 33) as described in the text. The same types of spectra are shown as in Fig. 2. Additionally, the interband contribution along the a axis is presented in (b) as a dotted blue line. The interband conductivity along the c axis is negligible in the shown energy range.

$$K(x,y) = \frac{i}{y} + \frac{y-x}{x}[\psi(1-ix+iy) - \psi(1+iy)]$$
$$+ \frac{y+x}{x}[\psi(1-ix-iy) - \psi(1-iy)],$$

and $\psi(x)$ is a digamma function.

All the ingredients to compute $\epsilon(\omega)$, except the impurity scattering rates $\gamma_{\sigma\, imp}$ and $\gamma_{\pi\, imp}$, which depend on the level and the nature of the impurities (substitutions, vacancies, dislocations, etc.), are provided by the *ab initio* local density approximation (LDA) calculations.

The spectra of the interband optical conductivity $\sigma_1^{IB}(\omega)$ obtained by different groups using the linear muffin tin orbital (LMTO),[31,32] full-potential linearized augmented plane wave (LAPW) (Ref. 33) and time-dependent density functional theory (DFT) (Ref. 34) methods, although showing some differences, are close to each other. In particular, we took the interband conductivity spectra, presented in Ref. 20

(Fig. 5) on the base of the full-potential LAPW method,[33] and computed the corresponding dielectric function $\epsilon_1^{IB}(\omega)$ by the KK transformation. The plasma frequencies reported by different groups[31–33] are also close to each other. We used the values $\omega_{p,a\sigma}=4.14$ eV, $\omega_{p,a\pi}=5.89$ eV, $\omega_{p,c\sigma}=0.68$ eV, and $\omega_{p,c\pi}=6.85$ eV.[21,33]

The *ab initio* calculated electron-phonon interaction functions were presented in Ref. 3. We used effective interaction functions for the two bands $\alpha_{tr}^2 F_\sigma(\omega) \equiv \alpha_{tr}^2 F_{\sigma\sigma}(\omega) + \alpha_{tr}^2 F_{\sigma\pi}(\omega)$ and $\alpha_{tr}^2 F_\pi(\omega) \equiv \alpha_{tr}^2 F_{\pi\pi}(\omega) + \alpha_{tr}^2 F_{\pi\sigma}(\omega)$ from the Refs. 3, 10, and 35. The electron-phonon coupling constant $\lambda_{tr}=2\int_0^\infty d\Omega \alpha_{tr}^2 F(\Omega)/\Omega$ is calculated to be about 1.1 for the σ bands and 0.55 for the π bands.

The calculated optical spectra are presented in Fig. 5. Here the scattering rates $\gamma_{\sigma imp}=12.4$ meV and $\gamma_{\pi imp}=85.6$ meV were taken; this choice is substantiated by the data fitting in the next section. Comparing Figs. 2 and 5, one can notice a remarkable overall agreement and even a reasonable quantitative match. We begin with the interband transitions. Both theoretical and experimental interband optical conductivities show a very strong anisotropy. Notably, the theory predicts no sizeable optical intensity along the *c* axis of the interband transitions below 4 eV, whereas there are two low-lying peaks at 0.35 and 2.4 eV for polarization parallel to the boron planes [see the dotted blue curve in Fig. 5(b)]. The 2.4 eV peak is due to a transition from the σ band to the π band close to the *M* point, where a van Hove singularity strongly enhances the density of states.[33] The peak at 0.35 eV corresponds to the transition between two close σ bands. The σ carriers are localized within the boron planes, which explains why these two transitions are optically very weak along the *c* axis.

Obviously, a strong peak in the experimental spectrum along the *a* axis at 2.6 eV matches the theoretical peak at 2.4 eV. The discrepancy in the peak position suggests that the separation between the σ band and π band is about 0.2 eV larger than predicted by the theory. It is remarkable,[36] that the same shift brings the results of the dHvA experiments[7] in MgB$_2$ close to theoretical predictions.[36,37]

According to the calculation, the $\sigma \rightarrow \sigma$ transition at 0.35 eV should manifest itself as a noticeable dip in the reflectivity spectrum [see inset in Fig. 5(a)]. Such a dip is not observed in the experimental spectra [Fig. 2(a)]. This peak may thus be shifted to even lower frequencies or be heavily overdamped. The first possibility is consistent with a shift of the σ bands with respect to the Fermi energy compared to the calculation, as proposed in Ref. 36. The broadening can be caused by the interaction with the conduction electrons, since the energy of this transition is within the width of the Drude peak.

A very intense sharp peak in the out-of-plane conductivity $\sigma_{1,c}(\omega)$ is expected around 5 eV.[20,31,34] This excitation was closely studied in Ref. 34 by the time-dependent DFT method. In the band picture, it comes from a transition between almost parallel bands. From the real-space point of view, this mode involves charge fluctuations between B and Mg sheets, dynamically screened by the intraband transitions.[34] As a consequence, a sharp plasma mode at 2.5 eV should emerge. Although 5 eV is beyond our experi-
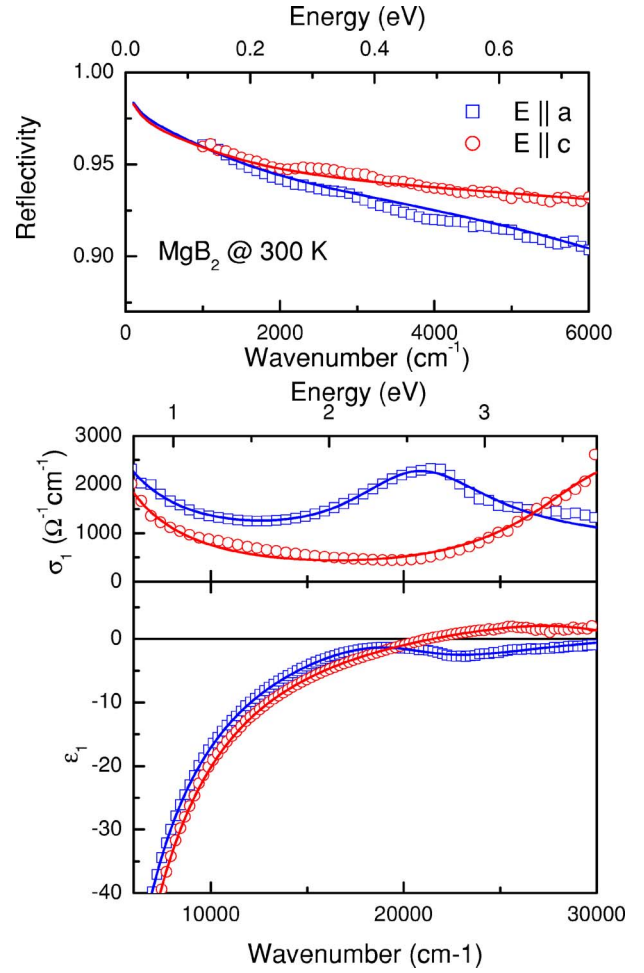

FIG. 6. (Color online) Experimental data (symbols) and the multiband fit (solid lines) of the reflectivity (a) and the dielectric function (b) along the *a* axis (blue) and the *c* axis (red).

mental range, there is a sizeable increase of $\sigma_{1,c}(\omega)$ above 3 eV, which can be a low-energy tail of this mode. The *c*-axis plasmon is at 2.6 eV, which is only slightly higher than the calculated value ($\sim$2.5 eV). This is in agreement with the inelastic x-ray scattering experiment.[12]

The shape and the width of the Drude peak agree well with the experiment, which suggests that phonons and impurities are the main factors of electron scattering. The integrated spectral weight $N_{eff}(\omega)$ grows faster according to the calculations, especially for the in-plane response. This indicates that the theory overestimates the value of the plasma frequency.

C. Two-band fitting of the spectra

The overall good agreement between the experimental and calculated data allows us to use the chosen model to fit the spectra, treating the plasma frequencies and scattering rates as adjustable parameters. We could achieve a satisfactory least-squares fit of reflectivity $R(\omega)$ in the midinfrared and $\epsilon_1(\omega)$ and $\sigma_1(\omega)$ at higher frequencies using formulas (6) and (7) as it is shown in Fig. 6. The corresponding parameter values are given in Table I. It turns out that leaving all four

plasma frequencies adjustable makes the fitting procedure underdetermined. Therefore, assuming the 2D nature of the σ band, we fixed the plasma frequencies of the σ band to the values given by *ab initio* calculations, and left only the total in-plane and c-axis plasma frequencies $\omega_{p,\text{tot}}^2 = \omega_{p,\sigma}^2 + \omega_{p,\pi}^2$ adjustable. Another assumption was that the *ab initio* calculations[3,10,35] correctly describe the electron-phonon functions $\alpha_{\text{tr}}^2 F_{\sigma,\pi}(\omega)$.

We modeled the interband conductivities by Lorentz oscillators ($\nu = a, c$)

$$\epsilon_\nu^{\text{IB}}(\omega) = \sum_i \frac{S_{\nu i}\omega_{\nu i}^2}{\omega_{\nu i}^2 - \omega^2 - \gamma_{\nu i}\omega} \qquad (8)$$

with adjustable frequency $\omega_{\nu i}$, oscillator strength $S_{\nu i}$, and width $\gamma_{\nu i}$. Keeping in mind the two interband peaks below 3 eV predicted by the theory, we put two Lorentzians to model $\epsilon_a^{\text{IB}}(\omega)$. Only one oscillator term above 3 eV was taken for $\epsilon_c^{\text{IB}}(\omega)$.

One can see that the bare plasma frequencies $\omega_{p,\sigma}$ and $\omega_{p,\pi}$ are almost the same and equal to 6.3 eV, which confirms our previous estimate based on the partial sum rule [Fig. 2(c)]. This value is much higher compared to previous reports[14,19–23] of 1.5–2.5 eV. Thus, the discrepancy with the theoretical value of 7 eV is likely to be much less than it was thought before. However, the current mismatch is not negligible since it results in about 20–25 % deviation of the Drude spectral weight. It is worth mentioning that the extremal orbit areas in the de Haas-van Alphen experiment[7] on both σ and π Fermi surfaces are also somewhat smaller than predicted by theory.[36,37] It was pointed out[36] that the discrepancy can be removed by a shift of the σ bands downward by about 115 meV and the π bands upward by 125 meV. This is in perfect agreement with our observation of the mismatch of 0.2 eV in the position of the 2.6 eV peak, as it is mentioned before. This also qualitatively explains the smaller value of the plasma frequency.

The impurity scattering rate in the π-band $\gamma_{\pi\,\text{imp}}$ is about 85 meV. Since the π electrons have rather strong optical spectral weight and a modest electron-phonon interaction, the absolute values of both $R_a(\omega)$ and $R_c(\omega)$ are quite sensitive to this parameter. In contrast, the value of $\gamma_{\sigma\,\text{imp}}$ does not significantly affect the spectra and cannot be accurately determined from the fit, because a large electron-phonon interaction in the σ band dominates the total scattering above 100 meV at 300 K. However, $\gamma_{\sigma\,\text{imp}}$ influences drastically the shape of the temperature-dependent in-plane dc resistivity $\rho_a(T) = 1/\sigma_{1,a}(\omega \to 0, T)$ curves, most notably the value of $\rho(300\ \text{K})/\rho(40\ \text{K})$ residual resistivity ratio (RRR), as can be seen from Fig. 7. A measurement[38] on a crystal grown in the same group under similar condition, showed RRR $\approx$ 5 along the a axis. Therefore we have chosen of $\gamma_{\sigma\,\text{imp}} = 12.4$ meV, which gives the same resistivity ratio (see Fig. 7). The assumption $\gamma_{\sigma\,\text{imp}} = \gamma_{\pi\,\text{imp}}$ gives RRR less than two, which strongly suggests that $\gamma_{\sigma\,\text{imp}}$ is actually several times smaller than $\gamma_{\pi\,\text{imp}}$. This agrees with the Raman study[39] on single crystals, where a relation $\gamma_{\pi\,\text{imp}}/\gamma_{\sigma\,\text{imp}} = 6-9$ was found, although the absolute values of the scattering rates are smaller than in our case.
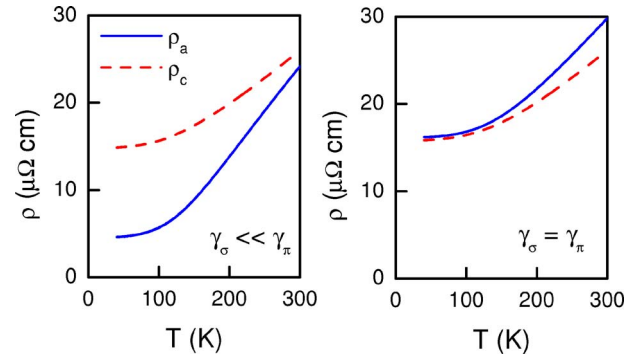

FIG. 7. (Color online) Temperature-dependent resistivity curves along the a axis (solid blue) and c axis (dashed red), calculated using the results of the fit of the optical data for $\gamma_{\pi\,\text{imp}} = 85.6$ meV and different values of the scattering rate in the σ band: $\gamma_{\sigma\,\text{imp}} = 12.4$ meV $\ll \gamma_{\pi\,\text{imp}}$(left) and $\gamma_{\sigma\,\text{imp}} = \gamma_{\pi\,\text{imp}}$ (right).

A disparity between the impurity scattering rates in the two bands and a small interband $\sigma \leftrightarrow \pi$ scattering were proposed in Ref. 21 to explain the surprisingly small dependence of T_c on the impurity level, not expected for a two-band superconductor. Microscopically, this can be explained by the fact that the electronic wave functions in σ bands are confined to the boron planes and not efficiently scattered by the magnesium vacancies and substitutions. On the other hand, the same defects strongly scatter the electron states in the 3D π bands. Our results support this conjecture.

The first Lorentz term for the a axis at 2.6 eV clearly corresponds to the discussed already interband transition. However, the second oscillator is extremely broad and it cannot be matched with a predicted interband peak at 0.35 eV. This probably means that this relatively weak peak is shifted and/or broadened so much that it cannot be identified in the optical spectrum. The second Lorentz term may thus describe the background formed by the tails of several broadened interband peaks.

D. The color of magnesium diboride

Finally we address a practical question: What is the color of MgB$_2$? The characterizations given in the literature varied significantly, ranging from the "golden" and "tan" to "silver-metallic," "black," and even "blue." Lee[40] has noticed that, depending on the polarization, "…the fresh surface of as-
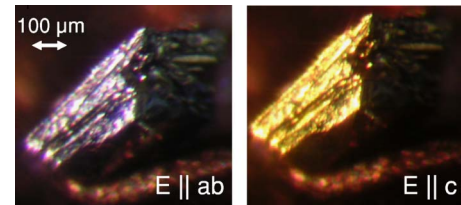

FIG. 8. (Color online) Two images of the same sample (*ac* plane) made in a polarized light: $E\|ab$ (left) and $E\|c$ (right). The sample looks golden for $E\|c$, due to a sharp reflectivity plasma edge at around 2.5 eV, while the plasma edge is smeared for $E\|ab$ by a strong $\sigma \to \pi$ interband transition at 2.6 eV.
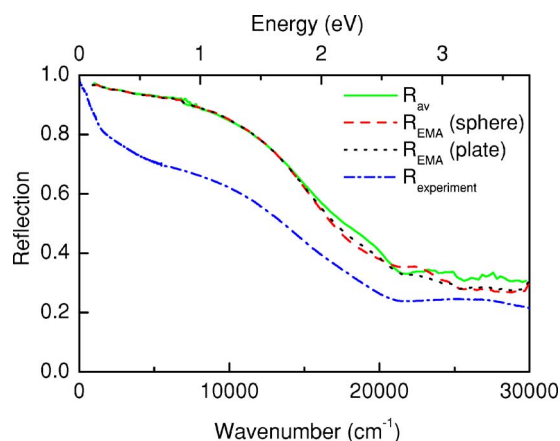
FIG. 9. (Color online) Reflectivity spectra of polycrystalline MgB$_2$ at 300 K. The spectra, calculated using the effective-medium approximation (spherical or platelike crystallites) and the direct reflectivity averaging, are compared with experimental spectrum from Ref. 20.
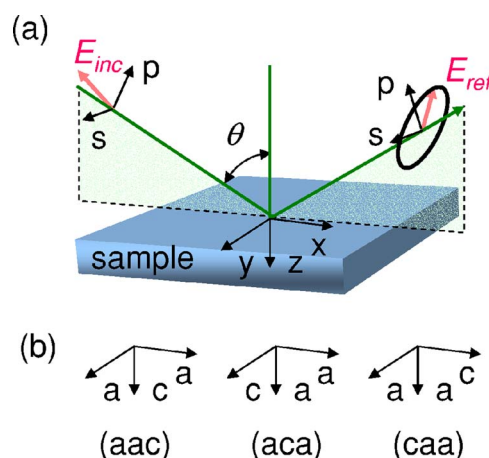

FIG. 10. (Color online) (a) The general configuration of ellipsometric experiment; (b) three specific sample orientations used in this paper.

grown crystals in the *ab* plane changes the color from silver to dark gray. In contrast, for the *ac* plane of the crystals a beautiful change of color from golden yellow to blue can be seen." Figure 8 shows the two images of the unpolished *ac* plane of the sample *S*1 for different polarizations of the incident white light. One can see that the sample spectacularly changes color from a blueish silver for *E*∥*ab* to the yellow for *E*∥*c*. The explanation comes naturally from the reflectivity curves shown in Fig. 2(a). For the *c*-axis polarization, it is a sharp plasma edge at about 2.5 eV, the same as of gold, which makes the sample yellow. For the *ab*-plane polarization, the plasma edge is smeared due to the strong interband transition at 2.6 eV. As a result, the reflectivity spectrum in the visible range (1.8–3.1 eV) is relatively flat with a maximum (stronger in sample *S*2) at ~2.8 eV which makes the color blue silver. Knowing the anisotropic spectra, we can predict the reflectivity shape of MgB$_2$ in the polycrystalline form. If the light wavelength λ is much larger than a typical grain size *l*, one can apply the effective-medium approximation (EMA) as prescribed in Ref. 41. In the short-wavelength limit λ≪*l*, it is more adequate to average directly the reflectivities along the two axes, as it was done in Ref. 23. In Fig. 9 both calculated curves $R_{EMA}(\omega)$ (for spherelike and platelike crystallites) and $R_{av}(\omega)=(2/3)R_{ab}(\omega)+(1/3)R_c(\omega)$ are shown, together with the spectrum on a polycrystal from our previous study.[20] Notably, $R_{EMA}(\omega)$ and $R_{av}(\omega)$ are close to each other and their overall shape in the visible range matches well the measured spectrum. The latter shows only a weak steplike feature near 2.5 eV, coming from the *c*-axis contribution,[23] which explains why the polycrystalline samples have typically black, or slightly tan, color. The absolute value of the experimental reflectivity from Ref. 20 is by 10–20% lower than the calculated one, which is likely caused by an overdamping of the π bands due to a much higher impurity level (presumably MgO) of the sample used.

V. CONCLUSIONS

We investigated anisotropic optical properties of MgB$_2$ single crystals of different purity at room temperature in the energy range 0.1–3.7 eV and compared them with the existing first principles calculations of the electronic structure and electron-phonon coupling. The analysis of the anisotropy allowed us to distinguish properties of the σ and π bands.

The total bare plasma frequencies along the in-plane and *c*-axis directions are almost the same and equal to 6.3 eV, which is much higher than the previously reported values. However, it is still smaller than the theoretical value of about 7 eV.

The shape of the Drude peak is well described by the electron scattering on phonons and impurities. The data suggest that the impurity scattering in the π bands is several times larger than in the σ bands in agreement with a proposal of Ref. 21, aimed to explain a surprisingly small dependence of the critical temperature on the sample purity. The electron-phonon interaction is stronger in the σ bands, in agreement with the theory[3] and de Haas-van Alphen experiments.[7]

The in-plane optical conductivity clearly shows an intense peak at 2.6 eV, which corresponds to a transition from the σ to the π band. It is higher by about 0.2 eV than the theoretical value. An interband peak due to the transitions between two close σ bands, expected to be at 0.35 eV, was not seen in the experiments which can be explained by an overdamping or a shift towards lower frequencies relative to the theoretical calculations.

The width of the Drude peak and the interband σ→π peak at 2.6 eV are very sensitive to the sample purity. This can partially explain the spread of the results of previous optical studies.

The two quantitative mismatches between the experiment and the theory, namely, (i) a smaller plasma frequency, and (ii) a higher by 0.2 eV energy of the 2.6 eV σ→π transition, tell us that the σ bands are probably shifted down and π bands are shifted up compared to the calculations, so that their relative shift is about 0.2 eV. Notably, the same conclusion was derived in Ref. 36 from the analysis of the dHvA measurements.[7]

The positions of the reflectivity plasma edges for two polarizations are very different (~2 eV for the *a* axis and ~2.5 eV for the *c* axis). This is caused by an additional
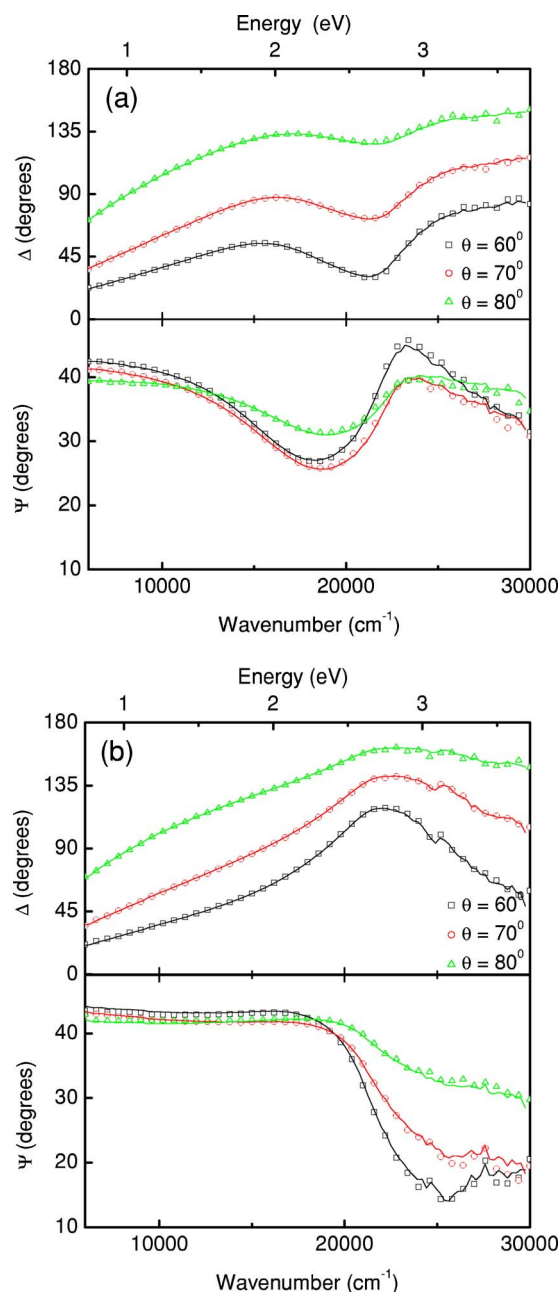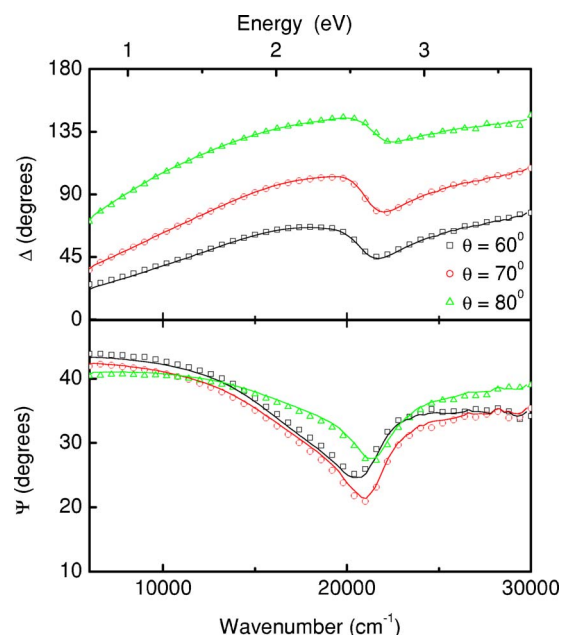
FIG. 12. (Color online) Ellipsometric spectra ψ and Δ for three angles of incidence (60°, 70°, and 80°) in the orientation (aac) [see Fig. 10(b)], measured on sample $S2$. Symbols are the measurement results, the solid lines correspond to the fit as described in the text.

APPENDIX: DETERMINATION OF $\epsilon_a(\omega)$ AND $\epsilon_c(\omega)$ FROM ELLIPSOMETRY

The general geometry of the ellipsometric experiment in the configuration "fixed analyzer (at 45°) - sample - rotating analyzer" is shown in Fig. 10(a). The axes x, y, and z are

FIG. 11. (Color online) Ellipsometric spectra ψ and Δ for three angles of incidence (60°, 70°, and 80°) in the orientations (aca)(a) (caa)(b) and [see Fig. 10(b)], measured on sample S1. Symbols are the measurement results, the solid lines correspond to the fit as described in the text.

screening of the intraband carriers by the interband transition at 2.6 eV, but not due to different ab-plane and c-axis bare plasma frequencies. As a result, the color of the sample depends on the polarization of the light: it is blueish-silver for E ∥ a and yellow for E ∥ c.
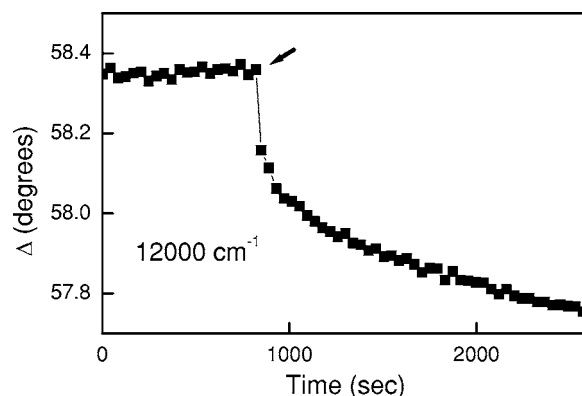
ACKNOWLEDGMENTS

FIG. 13. The effect of the exposure to the air on the optical properties of MgB$_2$. The time dependence of ellipsometric parameter Δ at 1.5 eV is shown [sample $S1$, geometry (caa), angle of incidence 70°]. Initially the sample was kept in a flow of dry nitrogen, which was switched off at the moment designated by the arrow.

assumed to be along the principal axes of the dielectric tensor of the sample. Ellipsometry provides two parameters ψ and Δ, related to the ratio of reflection coefficients for the p- and s-polarized light

$$\rho = r_p/r_s = \tan\psi \exp(i\Delta). \tag{A1}$$

r_p and r_s are given by the Fresnel formulas

$$r_p = \frac{\sqrt{1 - \varepsilon_z^{-1}\sin^2\theta} - \sqrt{\varepsilon_x}\cos\theta}{\sqrt{1 - \varepsilon_z^{-1}\sin^2\theta} + \sqrt{\varepsilon_x}\cos\theta}, \tag{A2}$$

$$r_s = \frac{\cos\theta - \sqrt{\varepsilon_y - \sin^2\theta}}{\cos\theta + \sqrt{\varepsilon_y - \sin^2\theta}}, \tag{A3}$$

where $\epsilon_\nu = \epsilon_{1\nu} + i\epsilon_{2\nu}$ ($\nu = x, y, z$) are the components of the complex dielectric tensor. In the case of optically uniaxial MgB$_2$ ($\epsilon_a = \epsilon_b \neq \epsilon_c$) three different orientations (xyz) are possible: (aac), (aca), and (caa) [see Fig. 10(b)].

On the sample $S1$ we did ellipsometry in the orientations (caa) and (aca). This yields four independent quantities ψ_{aca}, Δ_{aca}, ψ_{caa}, and Δ_{caa} at every photon energy and every chosen angle of incidence. Since each of these functions depends on the four values $\epsilon_{1,a}$, $\epsilon_{2,a}$, $\epsilon_{1,c}$, and $\epsilon_{2,c}$, the latter ones can be obtained by the numerical inversion of the four Fresnel equations. This procedure, when applied to three different angles of incidence (60°, 70°, and 80°), gave close results. In order to improve the accuracy of the output, we determined by the least squares fitting the values of $\epsilon_{1,a}$, $\epsilon_{2,a}$, $\epsilon_{1,c}$, and $\epsilon_{2,c}$ that render the best match to the measured ellipsometric parameters at all mentioned angles of incidence simultaneously. The experimental and fitting curves for the sample $S1$ for the orientations (aca) and (caa) are shown in Figs. 11(a) and 11(b), respectively. The second experiment was done on the sample $S2$ in the orientation (aac). The corresponding spectra of ψ_{aac} and Δ_{aac} for the same three angles of incidence are shown in Fig. 12 (as solid symbols). These data, taken alone, are not sufficient to extract both ϵ_a and ϵ_c independently. Since ψ_{aac} and Δ_{aac} are not very sensitive to the value of ϵ_c except close to the screened plasma frequency (according to Aspnes approximation),[42] we extracted $\epsilon_a(\omega)$, assuming that $\epsilon_c(\omega)$ is the same as the sample $S1$. One should realize that this introduces some uncertainty, because the samples $S1$ and $S2$ might have somewhat different c-axis dielectric functions. This uncertainty is negligible below 2 eV, but somewhat enhanced close to the c-axis plasmon at 2.6 eV. The best fit of ψ and Δ is given by the solid lines in Fig. 12.

Figure 13 shows that the ellipsometric parameters are affected immediately when a surface is exposed to air, due to the formation of a contamination layer. On the other hand, the flow of dry nitrogen efficiently preserves the surface quality. From the time dependence of the optical parameters one can estimate the error bars caused by the surface deterioration during the measurement. The corresponding analysis (not presented here) shows that they are much smaller than the difference between the optical spectra of the samples $S1$ and $S2$ (Fig. 3).

[1] J. Nagamatsu, N. Nakagawa, T. Muranaka, Y. Zenitani, and J. Akimitsu, Nature (London) **410**, 63 (2001).

[2] I. I. Mazin and V. P. Antropov, Physica C **385**, 49 (2003).

[3] Y. Kong, O. V. Dolgov, O. Jepsen, and O. K. Andersen, Phys. Rev. B **64**, 020501(R) (2001).

[4] S. L. Bud'ko, G. Lapertot, C. Petrovic, C. E. Cunningham, N. Anderson, and P. C. Canfield, Phys. Rev. Lett. **86**, 1877 (2001).

[5] D. G. Hinks, H. Claus, and J. D. Jorgensen, Nature (London) **411**, 6836 (2001).

[6] H. Uchiyama, K. M. Shen, S. Lee, A. Damascelli, D. H. Lu, D. L. Feng, Z.-X. Shen, and S. Tajima, Phys. Rev. Lett. **88**, 157002 (2002).

[7] E. A. Yelland, J. R. Cooper, A. Carrington, N. E. Hussey, P. J. Meeson, S. Lee, A. Yamamoto, and S. Tajima, Phys. Rev. Lett. **88**, 217002 (2002).

[8] Y. Wang, F. Bouquet, I. Sheikin, P. Toulemonde, B. Revaz, M. Eisterer, H. W. Weber, J. Hinderer, and A. Junod, J. Phys.: Condens. Matter **15**, 883 (2003).

[9] F. Bouquet, Y. Wang, I. Sheikin, T. Plackowski, A. Junod, S. Lee, and S. Tajima, Phys. Rev. Lett. **89**, 257001 (2002).

[10] A. A. Golubov, J. Kortus, O. V. Dolgov, O. Jepsen, Y. Kong, O. K. Andersen, B. J. Gibson, K. Ahn, and R. K. Kremer J. Phys.: Condens. Matter **14**, 1353 (2002).

[11] M. R. Eskildsen, M. Kugler, S. Tanaka, J. Jun, S. M. Kazakov, J. Karpinski, and O. Fischer, Phys. Rev. Lett. **89**, 187003 (2002).

[12] S. Galambosi, J. A. Soininen, A. Mattila, S. Huotari, S. Manninen, Gy. Vanko, N. D. Zhigadlo, J. Karpinski, and K. Hamalainen, Phys. Rev. B **71**, 060504(R) (2005).

[13] B. Gorshunov, C. A. Kuntscher, P. Haas, M. Dressel, F. P. Mena, A. B. Kuzmenko, D. van der Marel, T. Muranaka, and J. Akimitsu, Eur. Phys. J. B **21**, 159 (2001).

[14] R. A. Kaindl, M. A. Carnahan, J. Orenstein, D. S. Chemla, H. M. Christen, Hong-Ying Zhai, M. Paranthaman, and D. H. Lowndes, Phys. Rev. Lett. **88**, 027003 (2002).

[15] A. Pimenov, A. Loidl, and S. I. Krasnosvobodtsev, Phys. Rev. B **65**, 172502 (2002).

[16] J. H. Jung, K. W. Kim, H. J. Lee, M. W. Kim, T. W. Noh, W. N. Kang, Hyeong-Jin Kim, Eun-Mi Choi, C. U. Jung, and Sung-Ik Lee, Phys. Rev. B **65**, 052413 (2002).

[17] A. Perucchi, L. Degiorgi, J. Jun, M. Angst, and J. Karpinski, Phys. Rev. Lett. **89**, 097001 (2002).

[18] M. Ortolani, D. Di Castro, P. Postorino, I. Pallecchi, M. Monni, M. Putti, and P. Dore, Phys. Rev. B **71**, 172508 (2005).

[19] J. J. Tu, G. L. Carr, V. Perebeinos, C. C. Homes, M. Strongin, P. B. Allen, W. N. Kang, Eun-Mi Choi, Hyeong-Jin Kim, and Sung-Ik Lee, Phys. Rev. Lett. **87**, 277001 (2001).

[20] A. B. Kuzmenko, F. P. Mena, H. J. A. Molegraaf, D. van der Marel, B. Gorshunov, M. Dressel, I. I. Mazin, J. Kortus, O. V. Dolgov, T. Muranaka, and J. Akimitsu, Solid State Commun. **121**, 479 (2002).

[21] I. I. Mazin, O. K. Andersen, O. Jepsen, O. V. Dolgov, J. Kortus, A. A. Golubov, A. B. Kuzmenko, and D. van der Marel, Phys.

Rev. Lett. **89**, 107002 (2002).

[22] Mi-Ock Mun, Young Jin Kim, Yu Park, Jae Hoon Kim, S. H. Moon, H. N. Lee, H. G. Kim, and B. Oh, J. Supercond. **15**, 475 (2002).

[23] Y. Fudamoto and S. Lee, Phys. Rev. B **68**, 184514 (2003).

[24] F. Marsiglio, Phys. Rev. Lett. **87**, 247001 (2001).

[25] E. G. Maksimov, J. Kortus, O. V. Dolgov, and I. I. Mazin, Phys. Rev. Lett. **89**, 129703 (2002).

[26] D. Chvostova, V. Zelezny, L. Pajasova, A. Tarasenko, A. Plecenik, P. Kus, and L. Satrapinsky, Thin Solid Films **455**, 213 (2004).

[27] J. Karpinski, M. Angst, J. Jun, S. M. Kazakov, R. Puzniak, A. Wisniewski, J. Roos, H. Keller, A. Perucchi, L. Degiorgi, M. R. Eskildsen, P. Bordet, L. Vinnikov, and A. Mironov, Supercond. Sci. Technol. **16**, 221 (2002).

[28] A. B. Kuzmenko, Rev. Sci. Instrum. **76**, 083108 (2005).

[29] I. Bozovic, Phys. Rev. B **42**, 1969 (1990).

[30] O. V. Dolgov and S. V. Shulga, J. Supercond. **8**, 511 (1995).

[31] V. P. Antropov, K. D. Belashchenko, M. van Schilfgaarde, and S. N. Rashkeev, cond-mat/0107123 (unpublished).

[32] P. Ravindran, P. Vajeeston, R. Vidya, A. Kjekshus, and H. Fjellvag, Phys. Rev. B **64**, 224509 (2001).

[33] J. Kortus, I. I. Mazin, K. D. Belashchenko, V. P. Antropov, and L. L. Boyer, Phys. Rev. Lett. **86**, 4656 (2001).

[34] W. Ku, W. E. Pickett, R. T. Scalettar, and A. G. Eguiluz, Phys. Rev. Lett. **88**, 057001 (2002).

[35] O. V. Dolgov, Y. Kong, J. Kortus, and O. Jepsen (private communication).

[36] H. Rosner, J. M. An, W. E. Pickett, and S.-L. Drechsler, Phys. Rev. B **66**, 024521 (2002).

[37] I. I. Mazin and J. Kortus, Phys. Rev. B **65**, 180510(R) (2002).

[38] A. V. Sologubenko, J. Jun, S. M. Kazakov, J. Karpinski, and H. R. Ott, Phys. Rev. B **66**, 014504 (2002).

[39] J. W. Quilty, S. Lee, S. Tajima, and A. Yamanaka, Phys. Rev. Lett. **90**, 207006 (2003).

[40] S. Lee, Physica C **385**, 31 (2003).

[41] P. E. Sulewski, T. W. Noh, J. T. McWhirter, and A. J. Sievers, Phys. Rev. B **36**, 5735 (1987).

[42] D. E. Aspnes, J. Opt. Soc. Am. **70**, 1275 (1980).